Rev. Roum. Sci. Techn.– Électrotechn. et Énerg.
Vol. **61**, *4*, pp. 402–407, Bucarest, 2016

REAL TIME IMPLEMENTATION OF IMPROVED FRACTIONAL ORDER PROPORTIONAL-INTEGRAL CONTROLLER FOR GRID CONNECTED WIND ENERGY CONVERSION SYSTEM

ANTAR BEDDAR[1], HACENE BOUZEKRI[1], BADREDDINE BABES[2], HAMZA AFGHOUL[3]

Key words: Wind energy conversion, Fractional order proportional-integral (PI) controller, Switched controller, Switching algorithm, Grid connected.

This paper proposes a modified fractional order PI controller (MFO-PI) for grid connected variable speed wind energy conversion system (WECS). The proposed MFO-PI employs an integer integral action and fractional order integral action, and a supervisor to select the more suitable integral action looking to the working conditions. The parameters of the MFO-PI controller have been tuned using frequency method to realize the isodamping feature. The MFO-PI controller is used to guarantee maximum power extraction on the first and obtain power factor unity on the other hand. To investigate the efficiency of the proposed controller, an experimental bench has been carried out. The experimental results demonstrate the superiority of the proposed controller over integer order controllers for a wide range of wind speed.

1. INTRODUCTION

In the modern wind turbines, the permanent magnet synchronous generator (PMSG) plays an important role in variable speed wind energy conversion systems (WECSs), due to its high performance such as low volume weight, high power density, high torque to inertia ratio, high efficiency functioning at low rotational speed and no need to the gearbox [1–3]. WECS imposes regular maintenance due to the presence of unmodeled high-frequency oscillatory dynamics, which imposes a huge maintenance cost. Using robust control can reduce the maintenance cost [4–6]. In recent years, many nonlinear control methods have been developed for the WECS, such as fuzzy controller (FC) [7, 8], switched controller [9], robust adaptive neural controller [10], and so on. These approaches improve the control performance of the WECS from different aspects, but the complexity of these controllers imposes additional implementation and maintenance cost and need high online calculation ability and high human expert, which is far beyond the fixed parameters PI controller. On other hand; when the conventional PI controller is used, one can get good performance in steady state but a good closed-loop performance is very difficult to guarantee in different work conditions, where fast responses lead to large overshoots or small overshoots but with slow responses [6, 11]. These drawbacks are covered using fractional order PI controller (FO-PI) which has specific isodamping property; the flat phase around the gain crossover frequency ω_μ, which improves the conventional PI dynamics performances and earn more robustness to the parameters variations and external disturbances [11–13].

In our study, a modified fractional order PI controller (MFO-PI) has been proposed to control a WECS. The proposed MFO-PI composed of proportional gain, integral gain and two integrals actions (integer integral action (integration order =1) and fractional order integral action (integration order < 1)), in parallel with a supervisor involving switching rules, which is determined to select the more suitable integral action and connects it into the closed loop controlled system depending to the working conditions.

In more details, the supervisor has a defined band of the error (PMSG speed error/dc-bus voltage error). If the error is out of the desired band, the supervisor connects the fractional order integral action in the control loop, which means, the MFO-PI controller behaves as a FO-PI controller to bring the error to the desired band by guarantee fast response time and low overshoot, otherwise the supervisor connects the integer integral action to the control loop and the MFO-PI controller behaves as a conventional PI controller to ensure high steady state performance and eliminate the static error. Furthermore, the MFO-PI controller parameters have been tuned using frequency method to guarantee good steady state performance using integer integral, and earn more robustness to external disturbances and ensure fast response time without high overshoot using the fractional order integral action. Moreover, the MFO-PI controller was integrated in the speed loop of the vector control to ensure maximum power extraction on the first hand. On the other hand, the MFO-PI controller was integrated in the voltage loop of a direct power control to improve power quality and ensuring unity power factor.

The rest of the paper is organized as follows. Section 2 presents the WECS. Section 3 presents the MFO-PI controller with a procedure of design; Section 4 shows the experimental results and their interpretation, which conduct us to the Section 5 with the main conclusion.

2. WIND ENERGY CONVERSION SYSTEM

The WECS consists of three parts: mechanical part, electrical part and control part, whereas the mechanical part includes a wind turbine, which has been emulated using a dc motor with separate excitation. The mathematical model of the wind turbine is taking similar to [4], the electrical part includes 6.6 W PMSG connected to the grid (50 V, 50 Hz) via two back-to-back converters (machine side converter (MSC) and grid side converter (GSC)), and the control part was implemented with two real-time DSPACE1104 cards. The first card contains the improved current vector control [4] with the wind turbine model and wind profile. The direct power control (DPC) [8] was implemented in the second one to control the GSC as shown in Fig. 1

[1] Skikda University, Laboratoir d'Automatique Skikda, Electrical Engineering Department, Algeria, E-mail: antar_tech@hotmail.fr
[2] Setif university, Electrotechnics Department, LAS laboratory, Algeria
[3] M'sila University, Electronics Department, Algeria

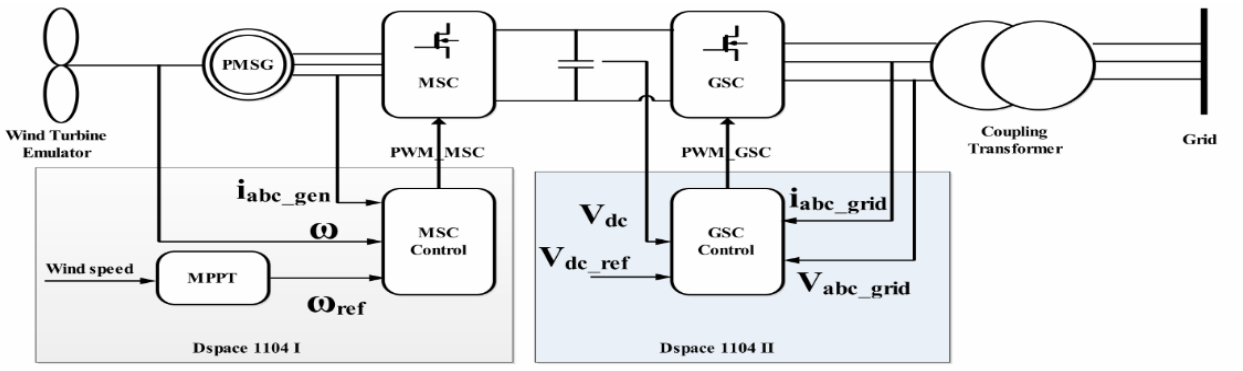

Fig. 1 – Wind energy conversion system.

2.1. WIND TURBINE MODEL

The wind turbine transforms the kinetic energy of the wind P_w to mechanical energy P_m. The relationship between them is the power coefficient of the turbine Cp given as [1, 4]:

$$P_m = \frac{1}{2} C_p(\lambda) \rho A V^3 = C_p(\lambda) P_w, \quad (1)$$

where ρ, *A*, *V*, λ are the air density (kg/m^3), the area swept by the rotor blades (m^2), the wind speed and the tip speed ratio (TSR) defined as [4, 6]:

$$\lambda = \frac{\Omega_t R_t}{V}, \quad (2)$$

where Ω_t is rotational speed and R_t is radius of the turbine blade [m].

For maximum power extraction, it is necessary that the TSR must reach its optimum value. This is possible by controlling the rotational PMSG speed so that it always rotates at the optimum speed. The PMSG optimum rotational speed can be extracted from Eq. (2) as

$$\Omega_{opt} = \frac{\lambda_{opt} V}{R_t}. \quad (3)$$

2.2. GENERATOR MODEL

The Park representation of the PMSG model is the commonly used, which its voltage equations are expressed by [6, 11]:

$$\begin{pmatrix} v_{sd} \\ v_{sq} \end{pmatrix} = -R_s \begin{pmatrix} i_{sd} \\ i_{sq} \end{pmatrix} - \frac{\mathrm{d}}{\mathrm{d}t} \begin{pmatrix} L_d i_{sd} \\ L_q i_{sq} \end{pmatrix} + \omega_e \begin{pmatrix} 0 & 1 \\ 1 & 0 \end{pmatrix} \begin{pmatrix} L_d i_{sd} + \varphi_f \\ L_q i_{sq} \end{pmatrix}, \quad (4)$$

where R_s, ω_e are the stator resistance and the generator electrical rotational speed respectively, $v_{sd,q}$, $i_{sd,q}$ are the d,q stator voltages and currents. $L_{d,q}$, φ_f Are the *d,q* axis inductances and magnetic flux. The mechanical equation of the PMSG is as follows

$$J \frac{\mathrm{d}\omega_e}{\mathrm{d}t} = T_w - T_m, \quad (5)$$

where *J*, ω_g is the inertia and mechanical speed of the PMSG; T_{wt} is the wind turbine torque.

3. **MODIFIED FRACTIONAL ORDER PI CONTROLLER**

In this paper, an improved fractional order PI controller was proposed to improve the system tracking and perturbation rejected performance in both transient and steady states. The MFO-PI controller implements proportional and integral gains with two integral actions in parallel with a supervisor (Switching Algorithm (SA)). Figure 2 shows the schematic of the proposed MFO-PI controller.

The MFO-PI controller has the following equation:

$$u(t) = k_p e(t) + k_i \left[(1 - k_s) \frac{\mathrm{d}^{-\alpha} e(t)}{\mathrm{d}t^{-\alpha}} + k_s \frac{\mathrm{d}^{-\alpha}}{\mathrm{d}t^{-\alpha}} \frac{\mathrm{d}^{-1+\alpha} e(t)}{\mathrm{d}t^{-1+\alpha}} \right]. \quad (6)$$

The MFO-PI controller output can be expressed in function of the supervisor output as follow:

$$\begin{aligned} u(t) &= k_p e(t) + k_i \frac{\mathrm{d}^{-\alpha} e(t)}{\mathrm{d}t^{-\alpha}} && (k_s = 0) \\ u(t) &= k_p e(t) + k_i \frac{\mathrm{d}^{-1+\alpha} \left(\frac{\mathrm{d}^{-\alpha} e(t)}{dt^{-\alpha}} \right)}{\mathrm{d}t^{-1+\alpha}} && (k_s = 1), \end{aligned} \quad (7)$$

where k_p, k_i are the proportional and integral gains respectively, α the fractional integration order and k_s is a two values [0 1] generated by the supervisor to select one integration action.

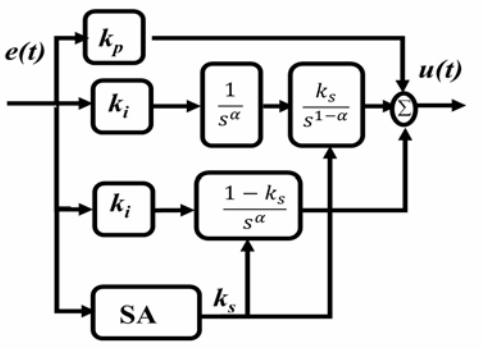

Fig. 2 – Modified fractional order PI controller.

3.1. CONTROLLER DESIGN

To design the MFO-PI controller, first the transfer function of the PMSG/dc-bus voltage is obtained as elaborated in [1, 4, 6]. Then, using the following equations, the MFO-PI controller can be designed.

In order to calculate the controller parameters (k_p, k_i and α), a frequency method was used to guarantee the system robustness [6]. The FO-PI controller has the following transfer function:

$$C_w = k_p + \frac{k_i}{s^\alpha}. \quad (8)$$

To guarantee the robustness of a linear fractional order controller the following criteria must be satisfied [4, 6]:

1) phase margin specification

$$\arg[G(\omega_c)] = \arg[C_w(j\omega_c)P(j\omega_c)] = -\pi + \phi_m, \quad (9)$$

where $C_w(j\omega_c), P(j\omega_c)$ are fractional order transfer function of the FO-PI controller and the PMSG speed/dc-bus voltage, respectively ω_c is the gain crossover frequency of the open loop system defined as follow:

$$|C_w(j\omega_c P(j\omega_c))|_{db} = 0, \quad (10)$$

and φ_m is the desired phase margin that ensures a desired stability margin level, which guarantees the robustness of the system against parameters uncertainties [6].

2) robustness against gain variations

$$\left(\frac{d(\arg(C_w(j\omega)P(j\omega)))}{d\omega}\right). \quad (11)$$

With the condition that the phase derivative at the frequency ω_c is zero, *i.e.*, the phase Bode plot is flat at the gain crossover frequency, the phase flat result in more robustness to the gain variation and uncertainties and the response time is faster because the large bandwidth. Moreover, the overshoots in a plan responses is almost the same even if the plan gain changes, so-called *isodamping* feature. One of the most significant features of fractional order controller is the possibility to realize the isodamping constraint with a compact transfer function [4, 13]. By solving the Eqs. (9), (10), (11), for given phase margin φ_m and, the controller parameters can be calculated.

3.2. OUSTALOUP CONTINUOUS APPROXIMATION

To implement the fractional order term s^α in simulation and practice it must be approximated by an integer transfer function, whereas a several methods have been developed. Oustaloup continuous approximation (OCA) is vastly used to approximate the fractional order s^α to integer transfer function [4, 14].

Oustaloup presented the approximation algorithm used when a frequency band of interest is given by $[\omega_b, \omega_h]$,

$$\left(\frac{s}{\omega_\mu}\right)^\alpha = H(s) = \left(\frac{\omega_\mu}{\omega_h}\right)^\alpha \prod_{k=-N}^{N}\left(\frac{1+s/\omega'_k}{1+s/\omega_k}\right), \quad (12)$$

where $\omega_\mu = \sqrt{\omega_b \omega_h}$,

$$\omega'_k = \omega_b\left(\frac{\omega_h}{\omega_b}\right)^{\frac{k+N+\frac{1}{2}-\frac{\alpha}{2}}{2N+1}}; \quad \omega_k = \omega_b\left(\frac{\omega_h}{\omega_b}\right)^{\frac{k+N+\frac{1}{2}+\frac{\alpha}{2}}{2N+1}}, \quad (13)$$

where ω'_k are the zeros, ω_k are the poles of rang k and $2N+1$ is the number of zeros or poles of the result integer transfer function [14]. When the number of poles and zeros $(2N+1)$ increases, it becomes difficult to implement these kinds of controllers in real domains, so, $N = 3$ was used to get seven poles and zeros.

3.3. SUPERVISOR

The supervisor has a defined band of the error and has the error as input, if the error is out of the desired band the k_s takes 0, otherwise k_s =1, as depicted in Fig. 3.

The supervisor is the responsible to select the more suitable controller, by looking to the error between the system output and its reference; if the error is out of the defined band, the MFO-PI must behave as a FO-PI controller to bring the error in the band and behaves as conventional PI controller when the error is in the desired band.

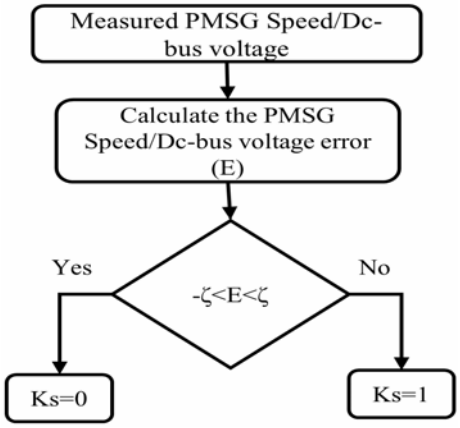

Fig. 3 – Supervisor.

3.4. STEPS TO DESIGN THE PROPOSED MFO-PI CONTROLLER

The steps to design the proposed controller are:

Step 1: calculate the proportional and integrator gains (k_p, k_i) and the real order of integration α of the FO-PI controller using the procedure in section 3.1.

Step 2: approximate the term $s^{-\alpha}$ to a rational transfer function using Oustaloup recursive approximation (to be implemented in simulation and practical tests) section 3.2.

Step 3: define the desired band for the PMSG speed/dc-bus voltage error, build the switching algorithm, in our case the PMSG speed error band was defined as [–6 rad/s, +6 rad/s] and for the dc-bus voltage was [–0.6V, +0.6V].

Step 4: build the MFO-PI controller for the PMSG speed loop and for the dc bus voltage loop.

4. **EXPERIMENTAL RESULTS**

As application of the proposed controller, wind energy conversion system is the system used to test the performance of the proposed MFO-PI controller.

The WECS consists of three parts: mechanical part, electrical part and control part. The mechanical part includes a wind turbine, which has been emulated using a dc motor with separate excitation. The electrical part includes a PMSG connected to the grid via back-to-back converters linked by a 2 200 μF, 1 800 V capacitor. A transformer was used for grid connection to allow the operation of the inverter with unity power factor. The control part was implemented with two real-time DSPACE1104 cards. The first card contains the improved current vector control with the wind turbine model and wind profile with sampling time of 60 μs, the direct power control was implemented in the second one with a sampling time equal to 50 μs. The rotor position is obtained through an encoder giving 1500 pulses per revolution. The experimental results are recorded using the control desk interface, whereas the voltage and current waveforms are captured using numerical oscilloscope.

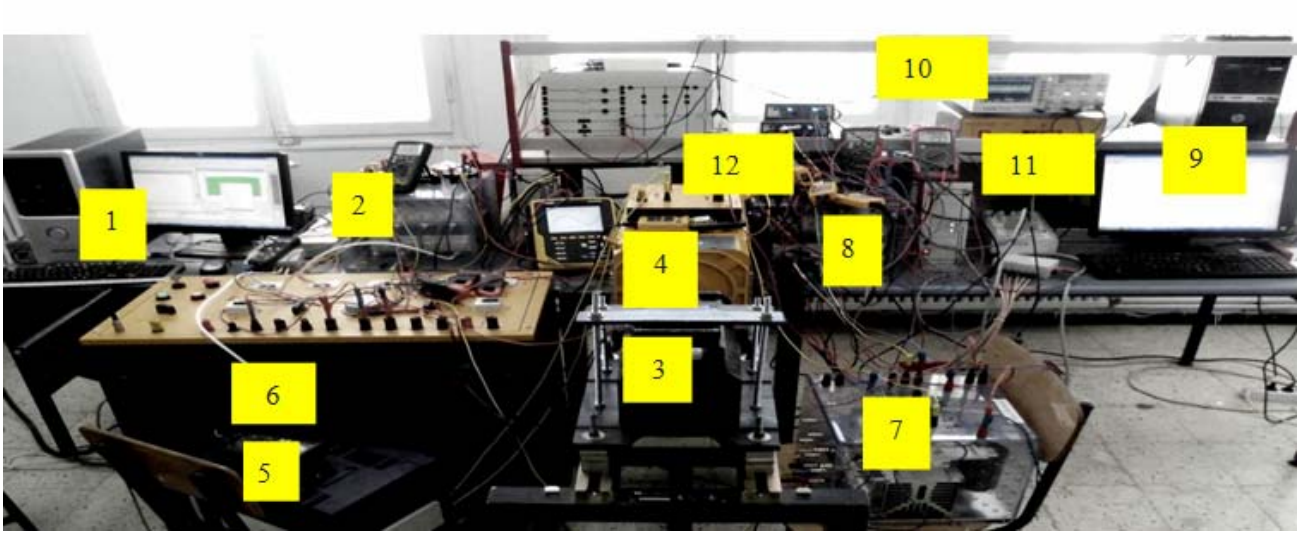

Fig. 4 – Experimental setup for WECS: 1. – PC with first DSPACE; 2 – machine side converter; 3 – PMSG; 4 – DC motor; 5 – separate excitation; 6 – transformer; 7 – dc/dc converter; 8 – Grid side converter; 9 – PC with second DSPACE; 10 – numerical scope; 11 – speed sensor; 12 – voltage and currents sensors.

4.1. TRACKING PERFORMANCE USING CONVENTIONAL PI CONTROLLER

Figures 5–7 show the response of the system with MPPT controller based on the conventional PI controller. From Fig. 6, It is clear that the PMSG speed has an overshoot in track its optimal value, which leads to losses in the power extraction as seen in Fig. 7, the power coefficient C_p is far from its optimum value.

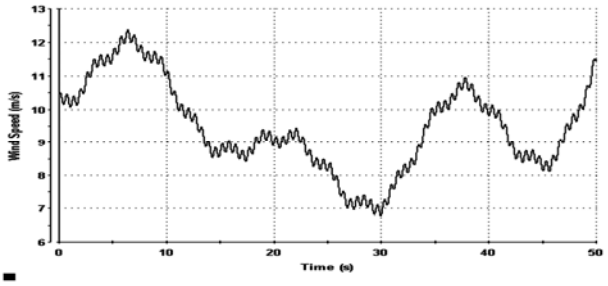

Fig. 5 – Wind profil speed.

4.2. TRACKING PERFORMANCE USING MFO-PI CONTROLLER

Figures 8–10 show the response of the system with maximum power point tracking (MPPT) controller based MFO-PI for the same wind speed profile. From Fig. 9 It is noticed that the PMSG speed tracks perfectly its optimal value for all wind speeds. In normal condition, when the PMSG speed is close to its reference value (in the desired band), the supervisor connects the integral of order 1 to the loop control to eliminate the steady state error that guarantees optimal power coefficient (k_s= 0). In the presence of strong variation of wind speed the PMSG speed departs abnormally from its reference value, the supervisor detects the new work condition and evaluates the new error and connects the fractional order integral to the control loop to deal with this abnormal condition (k_s= 1), as seen in Fig. 11. The MFO-PI controller drives the PMSG speed to the desired band in short time that lead to maximum power extraction. As seen in Fig. 10 the C_p is close to its optimum value using MFO-PI under wide range of wind speed, these results confirm the robustness and the superiority of the proposed MFO-PI against the conventional controllers.

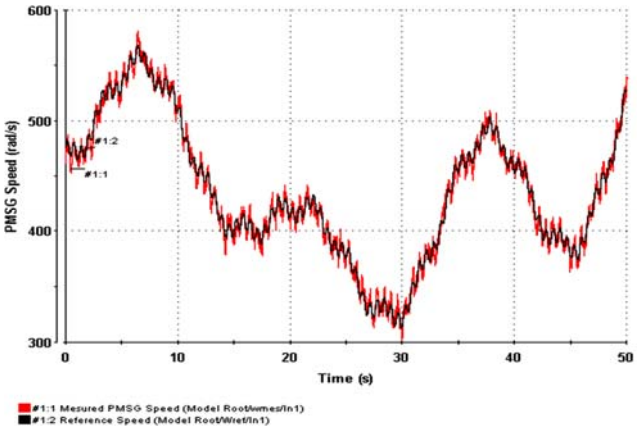

Fig. 6 – PMSG Speed using conventional PI controller.

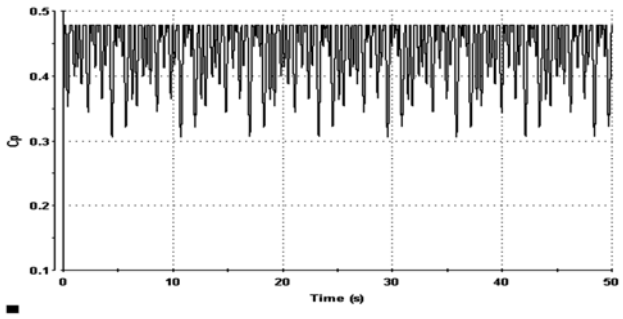

Fig. 7 – Power coefficient using conventional PI controller.

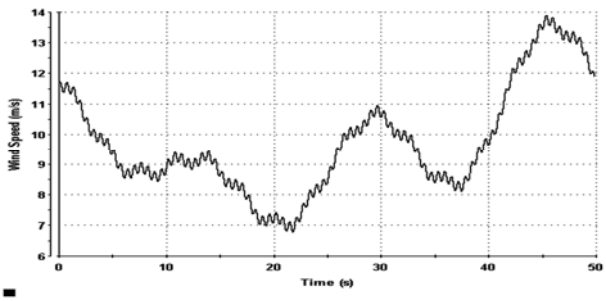

Fig. 8 – Wind speed profile.

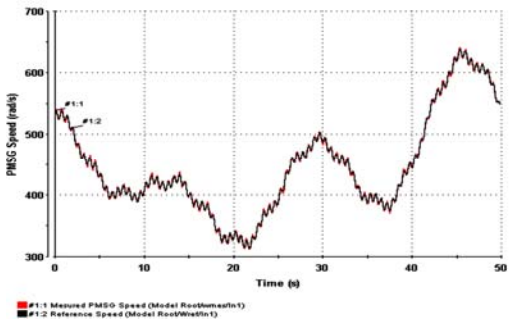

Fig. 9 – PMSG speed using MFO-PI controller.

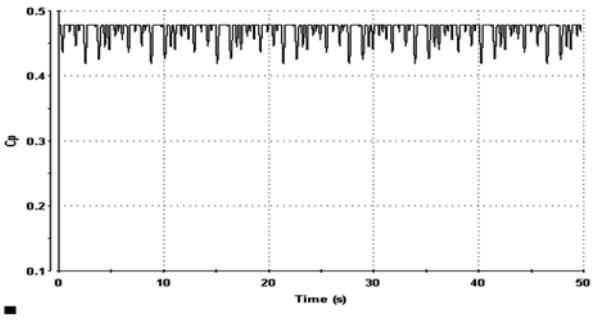

Fig. 10 – Power coefficient using MFO-PI controller.

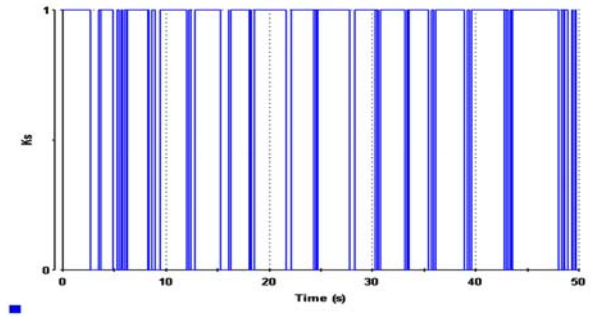

Fig. 11 – Switching algorithm output (ks).

4.3. GRID CONNECTION PERFORMANCE USING MFO-PI CONTROLLER

The power extracted from the wind is transferred to the grid via the dc link capacitor voltage. Figures 12–13 show the current injected to the grid for variable speed wind profile, it is clear that the dc link voltage is stable and remains the same with minimal ripple and the grid voltage is constant. When the dc bus voltage is closed to its reference value (in the desired band), the MFO-PI behaves as conventional PI controller in the control loop. When the conventional PI controller cannot keep the dc-bus voltage close to its reference value because of the unexpected wind speed change, the supervisor changes the integration order and the MFO-PI behaves as FO-PI controller to deal with this new condition.

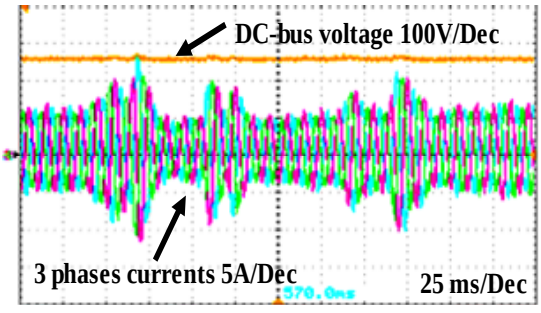

Fig. 12 – Dc-bus voltage and three phases current injected to the grid.

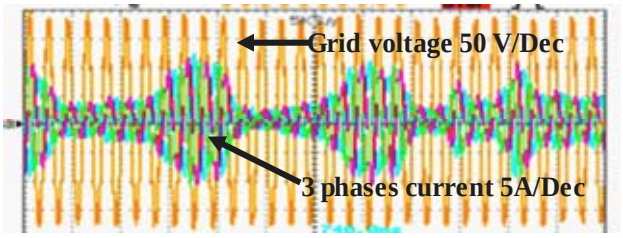

Fig. 13 – Grid voltage and three phases current injected to the grid.

A step transition of wind speed from 2 m/s to 7 m/s is applied. In this case, the three phase currents are sinusoidal and their amplitude is increased with the wind speed. Observe that the dc bus voltage is constant under wind variation as shown in Fig. 14, which proves the robustness of the MFO-PI controller. Moreover, in Fig. 15 the generated PMSG active power shifts very quickly with the wind change and is transferred to the grid with minimum losses in the converter and the reactive power is kept to zero. The grid-side current THD of the grid current is approximately 8.8 % using the conventional PI controller and 4.2 % using the MFO-PI controller, which respects the standards imposed by *IEEE* as shown in Figs. 16 and 17.

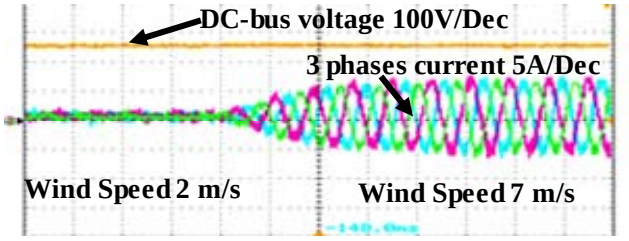

Fig. 14 –Dc-bus voltage and three phases current injected to the grid under wind step change.

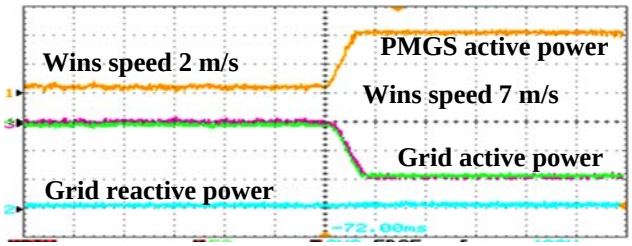

Fig. 15 – Grid active and reactive power under step wind change.

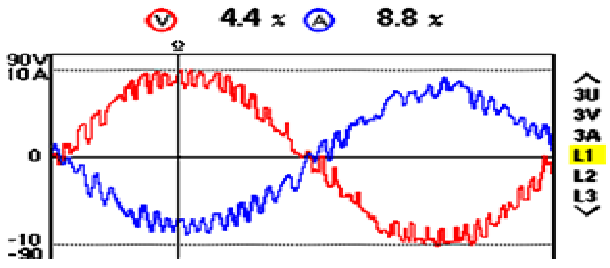

Fig. 16 – Current grid THD using PI controller.

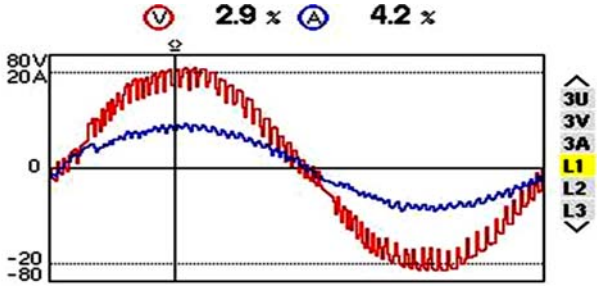

Fig. 17 – Current grid THD using MFO-PI controller.

5. **CONCLUSION**

In this paper, a modified fractional order PI controller (MFO-PI) for variable speed WECS is proposed. The MFO-PI combines fractional order integral action and integer order integral action, and together with the supervisor was integrated to the current vector control algorithm for maximum power extraction by controlling the PMSG speed to track its optimal reference generated by the MPPT. Indeed, the MFO-PI was integrated to direct power control (DPC) algorithm, which was designed to regulate the dc-bus voltage by keeping the capacitor voltage oscillating around a desired reference. The effectiveness of the proposed control schemes has been tested experimentally in laboratory. Whereas a wind turbine emulator based on a dc motor has been realized to drive an industrial PMSG connected to the grid via back-to-back converters linked by a dc capacitor. The experimental results shown that both improved vector control and DPC algorithms can achieve fast response time, very good tracking and robust performances, maximum power extraction with maximum C_p error 15 % and low currents THD 4.2 %.

Appendix A

Wind turbine parameters

$C_{p\_\max} = 0.7, \lambda_{opt} = 8.1, R_t = 1.02$ m, $\rho = 7{,}225$ kg/m^3

PMSG parameters

$R_s = 1.6\ \Omega$, $L_d = L_q = 0.006365$ H, $\varphi_f = 0.1852$ Wb,

$p = 8$, $J = 18.5 \cdot 10^{-5}$ kgm^2, $P = 6.6$ kW, $V = 380$ V

MFO-PI controller parameters for MSC

k_p=18.6, k_i=12.3, $\alpha = 0.6$, φ_m=45°, error desired band for the PMSG speed [–6 rad/s, +6 rad/s].

MFO-PI controller parameters for GSC

$k_p = 56.8$, $k_i = 22.12$, $\alpha = 0.7$, $\varphi_m = 45°$, error desired band for the dc bus voltage [–0.6V, +0.6 V].

Approximation parameters

$\omega_b = 10^{-4}, \omega_h = 10^4$, $N = 3$.

Received on November 5, 2015

REFERENCES

1. B. Antar, B. Hacene, B. Badredine, A. Hamza, *Experimental enhancement of fuzzy fractional order PI+I controller of grid connected variable speed wind energy conversion system*, Energy Conv and Manag, **123**, pp. 569–580 (2016).
2. M. Doumi, A. Aissaoui, A. Tahour, M. Abid, *Commande Adaptative d'un Système Éolien*, Rev. Roum. Sci. Techn. – Électrotechn. et Énerg, **60**, *1*, pp. 99–110 (2015).
3. A. Kerboua , M Abid, *Hybrid Fuzzy Sliding Mode Control of a Doubly-Fed Induction Generator in Wind Turbines*, Rev. Roum. Sci. Techn. – Électrotechn. et Énerg., **57**, *4*, pp. 412–421 (2012).
4. A. Beddar, H. Bouzekri, B. Babes, H. Afghoul, *Fractional order PI controller for grid connected wind energy conversion system*, 4th International Conference on Electrical Engineering (ICEE), Boumerdes, pp.1–6 (2015).
5. Maryam Falah Nezhadaneini, M. Karimi, Nasser Yousefi, *A novel metaheuristic approach to solve unit commitment problem in the presence of wind farms*, Rev. Roum. Sci. Techn. – Électrotechn. Et Énerg, **60**, *3*, pp. 253–262 (2015).
6. G. Shahab, T. Ahmadreza, A. Javad, *Application of Fractional Calculus Theory to Robust Controller Design for Wind Turbine Generators*, IEEE transactions on energy conversion, **29**, *3*, pp. 780–787 (2014).
7. A. Zebar, A. Hamouda, K. Zehar, *Impact of the location of fuzzy controlled static VAR compensator on the power system transient stability improvement in presence of distributed wind generation*, Rev. Roum. Sci. Techn. – Électrotechn. et Énerg, **15**, *4*, pp. 426–436 (2015).
8. A. Hamza, K. Fateh, C. Djamel, A. Beddar, *Design and real time implementation of fuzzy switched controller for single phase active power filter*, ISA Transactions, doi.org/10.1016/j.isatra.2015.07.008, (2015).
9. U. Lanka, W. Keigo, I. Kiyotaka , K. Kazuo, *Control of Underactuated Manipulators using Fuzzy Logic Based Switching Controller*. Journal of Intelligent and Robotic Systems, **38**, pp. 155–173 (2003).
10. Y. Lei, F. Shumin, S. Lining, H. Jun, Y. Gang, *Design of Robust Adaptive Neural Switching Controller for Robotic Manipulators with Uncertainty and Disturbances*, J. Intell. Robot. Syst., doi 10.1007/s10846-013-0008-3.
11. R. Melício, V.M.F. Mendes, J.P.S. Catalão, *A Pitch Control Malfunction Analysis for Wind Turbines with Permanent Magnet Synchronous Generator and Full-power Converters: Proportional Integral Versus Fractional-order Controllers*, Electric Power Components and Systems, **38**, *4* (2010).
12. M. Sedraoui, D. Boudjehem, *Robust fractional order controller based on improved particle swarm optimization algorithm for the wind turbine equipped with a doubly fed asynchronous machine*, Proceedings of the Institution of Mechanical Engineers, Part I: Journal of Systems and Control Engineering, **226**, *9*, pp. 1274–1286 (2012).
13. M. Tavazoei, *From Traditional to Fractional PI Control*, IEEE Industrial electronics magazine, **6**, *3*, pp. 41–51 (2012).
14. A. Oustaloup, F. Levron, F. Nanot, B. Mathieu, *Frequency-band complex non integer differentiator: characterization and synthesis*, IEEE Trans Circuits and Systems I: Fundamental Theory and Applications, **47**, *1*, pp. 25–40 (2000).